Discrete Exterior Calculus Discretization of the Navier-Stokes Equations

Mamdouh M. Mohamed (Post-doc, ME, PSE Division)
Anil N. Hirani (Dept. of Math, UIUC)
Ravi Samtaney (ME, PSE Division)

KAUST
King Abdullah University of Science and Technology

fps
Discovery through simulation

Jan 10, 2017

Outline

1. Motivation
2. What is DEC?
3. DEC discretization of incompressible Navier-Stokes equations.
4. Hodge star operators for non-Delaunay meshes.
5. Hybrid discrete Hodge star operator.
6. Proposed DEC discretization of MHD equations.
7. Conclusions.

KAUST
King Abdullah University of Science and Technology

Motivation

Fidelity measures of a numerical discretization method.

- Numerical fidelity: **convergence** and **stability** indicate how well the mathematics of the PDE are represented by the numerical method.
- Physical fidelity: how well the physics of the system are preserved by the numerical method.
- Preserving the key physical quantities during the numerical solution is important to avoid non-physical numerical artefacts.

Motivation

Key physical quantities to preserve:

- Conservation of primary quantities: mass, momentum and energy.
- Conservation of secondary quantities:[J. Perot, Annu. Rev. Fluid Mech. 2011]
  - Vorticity: e.g. important for turbulence and shallow water simulations.
  - Kinetic energy: large-eddy simulation of turbulent flow.
  - Entropy: compressible flow simulations.

The covolume method

- The covolume method, originally introduced by Nicolaides (1989) and Hall et al. (1991), is a low order method that is free of spurious modes.
- The covolume method convergence was estimated by Nicolaides (1992) to be of second order rate for structured/semi-structured meshes and first order accurate otherwise.

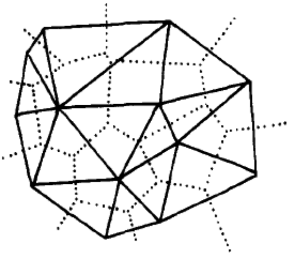

The covolume method

- The local/global conservation properties of the covolume method were later revealed by Perot (2000).
- The conservative behavior of the covolume method is attributed to the discrete differential operators that mimic the behavior of their smooth counterparts.
- The resulting discrete system can be manipulated into discrete conservation statements for key physical quantities.
- The covolume method conserves mass, momentum, vorticity and kinetic energy.

What is Exterior Calculus?

- Exterior Calculus is an alternative language to Vector Calculus in describing mathematical formula in a more generalized arbitrary order sense.
- Instead of scalars, vectors and tensors in Vector Calculus, we have $k-$forms in Exterior Calculus.
- For the differential operators:
  - (d) is equivalent to (∇)
  - $(*\mathrm{d})$ is equivalent to $(\nabla\times)$
  - $(*\mathrm{d}*)$ is equivalent to $(\nabla\cdot)$
  - $(.\wedge.)$ is equivalent to $(.\times.)$

Why DEC?

1- Both Exterior Calculus and its discretization (DEC) are formulated for curved surfaces.

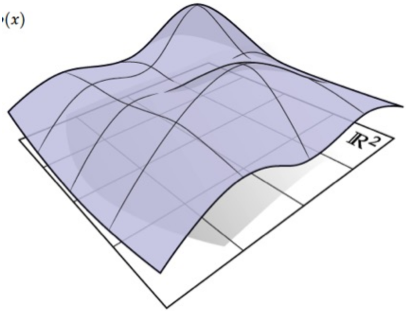

A DEC discretization of a physical problem is applicable to both flat and curved domains without any modifications.

Why DEC?

2- The DEC operators are generally mimetic.

Mimetic behavior means that the discrete operators follow the same rules/identities governing the smooth operators (i.e. $\nabla \cdot \nabla \times \boldsymbol{\psi} = 0$).

The mimetic discrete operators usually result in a conservative discretization that conserves many of the primary and secondary physical quantities in the governing equations.

This will be further demonstrated in the incompressible Navier Stokes discretization.

KAUST
King Abdullah University of Science and Technology

Incompressible Navier-Stokes equations:

$$\boxed{\begin{aligned} \frac{\partial \mathbf{u}}{\partial t} - \mu \Delta \mathbf{u} + (\mathbf{u}.\nabla)\mathbf{u} + \nabla p = 0 \\ \nabla.\mathbf{u} = 0 \end{aligned}}$$

Using the vector identities:

$$\Delta \mathbf{u} = \nabla(\nabla.\mathbf{u}) - \nabla \times (\nabla \times \mathbf{u})$$

$$(\mathbf{u}.\nabla)\mathbf{u} = \frac{1}{2}\nabla(\mathbf{u}.\mathbf{u}) - \mathbf{u} \times (\nabla \times \mathbf{u})$$

Define the dynamic pressure: $p^d = p + \frac{1}{2}(\mathbf{u}.\mathbf{u})$

$$\boxed{\begin{aligned} &\frac{\partial \mathbf{u}}{\partial t} + \mu \nabla \times \nabla \times \mathbf{u} - \mathbf{u} \times (\nabla \times \mathbf{u}) + \nabla p^d = 0 \\ &\nabla.\mathbf{u} = 0 \end{aligned}}$$

Incompressible Navier-Stokes equations in exterior calculus notation:

$$\boxed{\begin{aligned}&\frac{\partial \mathbf{u}}{\partial t} + \mu \nabla \times \nabla \times \mathbf{u} - \mathbf{u} \times (\nabla \times \mathbf{u}) + \nabla p^d = 0\\ &\nabla . \mathbf{u} = 0\end{aligned}}$$

For any vector field $\mathbf{u}$ and a scalar field f:

$$\begin{aligned}(\nabla \times \nabla \times \mathbf{u})^\flat &= (-1)^{N+1} * \mathrm{d} * \mathrm{d}\mathbf{u}^\flat,\\ (\mathbf{u} \times (\nabla \times \mathbf{u}))^\flat &= (-1)^{N+1} * (\mathbf{u}^\flat \wedge *\mathrm{d}\mathbf{u}^\flat),\\ (\nabla . \mathbf{u})^\flat &= *\mathrm{d} * \mathbf{u}^\flat,\\ (\nabla f)^\flat &= \mathrm{d}f\end{aligned}$$

$$\boxed{\begin{aligned}&\frac{\partial \mathbf{u}^\flat}{\partial t} + (-1)^{N+1}\mu * \mathrm{d} * \mathrm{d}\mathbf{u}^\flat + (-1)^{N+2} * (\mathbf{u}^\flat \wedge *\mathrm{d}\mathbf{u}^\flat) + \mathrm{d}p^d = 0,\\ &* \mathrm{d} * \mathbf{u}^\flat = 0\end{aligned}}$$

An alternative derivation:

Starting from Navier-Stokes equation in coordinate invariant form (See Abraham, Marsden, Ratiu, "Manifolds, Tensor Analysis and Applications")

$$\boxed{\frac{\partial \mathbf{u}^\flat}{\partial t} + \mu(\delta \mathrm{d} + \mathrm{d}\delta)\mathbf{u}^\flat + \pounds_{\mathbf{u}}\mathbf{u}^\flat - \frac{1}{2}\mathrm{d}(\mathbf{u}^\flat(\mathbf{u})) + \mathrm{d}p = 0}$$

where δ is the codifferential operator defined as $\delta = (-1)^{N(k-1)+1} * \mathrm{d} *$.

Using Cartan homotopy formula:

$$\pounds_{\mathbf{u}}\mathbf{u}^\flat = \mathrm{d}i_{\mathbf{u}}\mathbf{u}^\flat + i_{\mathbf{u}}\mathrm{d}\mathbf{u}^\flat = \mathrm{d}(\mathbf{u}^\flat(\mathbf{u})) + i_{\mathbf{u}}\mathrm{d}\mathbf{u}^\flat$$

$$\boxed{\frac{\partial \mathbf{u}^\flat}{\partial t} + \mu\delta\mathrm{d}\mathbf{u}^\flat + i_{\mathbf{u}}\mathrm{d}\mathbf{u}^\flat + \frac{1}{2}\mathrm{d}(\mathbf{u}^\flat(\mathbf{u})) + \mathrm{d}p = 0.}$$

An alternative derivation: Cont.

$$\boxed{\frac{\partial \mathbf{u}^\flat}{\partial t} + \mu\delta\mathrm{d}\mathbf{u}^\flat + i_{\mathbf{u}}\mathrm{d}\mathbf{u}^\flat + \frac{1}{2}\mathrm{d}(\mathbf{u}^\flat(\mathbf{u})) + \mathrm{d}p = 0.}$$

- Defining the dynamic pressure 0-form as $p^d = p + \frac{1}{2}(\mathbf{u}^\flat(\mathbf{u}))$.
- Substitute with $\delta = (-1)^{N+1} * \mathrm{d} *$.
- Substitute for the contraction with [A. Hirani, PhD Dissertation, Caltech (2003)]

$$i_{\mathbf{x}}\alpha = (-1)^{k(N-k)} * (*\alpha \wedge \mathbf{x}^\flat)$$

$$\boxed{\frac{\partial \mathbf{u}^\flat}{\partial t} + (-1)^{N+1}\mu * \mathrm{d} * \mathrm{d}\mathbf{u}^\flat + (-1)^{N-2} * (\mathbf{u}^\flat \wedge *\mathrm{d}\mathbf{u}^\flat) + \mathrm{d}p^d = 0.}$$

Applying the exterior derivative (d) to the above equation

$$\boxed{\frac{\partial \mathrm{d}\mathbf{u}^\flat}{\partial t} + (-1)^{N+1}\mu\mathrm{d} * \mathrm{d} * \mathrm{d}\mathbf{u}^\flat + (-1)^{N}\mathrm{d} * (\mathbf{u}^\flat \wedge *\mathrm{d}\mathbf{u}^\flat) = 0.}$$

Domain discretization:

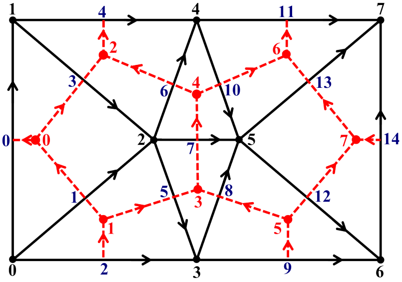

- The domain Ω is approximated by the simplicial complex K.
- A k-simplex is denoted by $\sigma^k = [v_0, \ldots, v_k] \in K$.
- The circumcentric dual to the simplicial complex K is the dual complex $\star K$.
- For a primal k-simplex $\sigma^k \in K$, its dual is an $(N-k)$-cell denoted by $\star\sigma^k \in \star K$

- Discrete differential forms: a discrete form can be thought as the integration of the smooth form over a discrete mesh object; i.e. line, area or volume.
- For example, for the smooth velocity 1-form $\mathbf{u}^\flat$, its discretization can be defined:
    - on primal edges σ^1 as $v = \int_{\sigma^1} \mathbf{u} \, d\mathbf{l}$.
    - on dual edges $\star\sigma^1$ as $u = \int_{\star\sigma^1} \mathbf{u} \, d\mathbf{l}$.

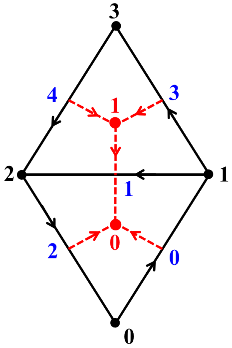

Discrete Exterior Calculus:

The space of discrete k-forms defined on primal and dual mesh complexes is denoted by $C^k(K)$ and $D^k(\star K)$, respectively.

$$
\begin{tikzcd}
C^0(K) \arrow[r, "\mathrm{d}_0"] \arrow[d, "*_0"] & C^1(K) \arrow[r, "\mathrm{d}_1"] \arrow[d, "*_1"] & C^2(K) \arrow[d, "*_2"] \\
D^2(\star K) & D^1(\star K) \arrow[l, "-\mathrm{d}_0^T"'] & D^0(\star K) \arrow[l, "\mathrm{d}_1^T"']
\end{tikzcd}
$$

$$
\begin{tikzcd}
C^0(K) \arrow[r, "\mathrm{d}_0"] \arrow[d, "*_0"] & C^1(K) \arrow[r, "\mathrm{d}_1"] \arrow[d, "*_1"] & C^2(K) \arrow[r, "\mathrm{d}_2"] \arrow[d, "*_2"] & C^3(K) \arrow[d, "*_3"] \\
D^3(\star K) & D^2(\star K) \arrow[l, "\mathrm{d}_0^T"'] & D^1(\star K) \arrow[l, "\mathrm{d}_1^T"'] & D^0(\star K) \arrow[l, "\mathrm{d}_2^T"']
\end{tikzcd}
$$

Examples of DEC operators:

$$d_0\beta = \begin{bmatrix} -1 & 1 & 0 & 0 \\ 0 & -1 & 1 & 0 \\ 1 & 0 & -1 & 0 \\ 0 & -1 & 0 & 1 \\ 0 & 0 & 1 & -1 \end{bmatrix} \begin{bmatrix} \beta_0 \\ \beta_1 \\ \beta_2 \\ \beta_3 \end{bmatrix}$$

$$d_1 = \begin{bmatrix} 1 & 1 & 1 & 0 & 0 \\ 0 & -1 & 0 & 1 & 1 \end{bmatrix}$$

$$\star_1 = \begin{bmatrix} \frac{|\star\sigma_0^1|}{|\sigma_0^1|} & 0 & 0 & 0 & 0 \\ 0 & \frac{|\star\sigma_1^1|}{|\sigma_1^1|} & 0 & 0 & 0 \\ 0 & 0 & \frac{|\star\sigma_2^1|}{|\sigma_2^1|} & 0 & 0 \\ 0 & 0 & 0 & \frac{|\star\sigma_3^1|}{|\sigma_3^1|} & 0 \\ 0 & 0 & 0 & 0 & \frac{|\star\sigma_4^1|}{|\sigma_4^1|} \end{bmatrix}$$

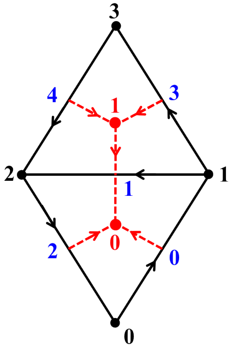

Discrete Exterior Calculus

For the discrete wedge product, we use the definition in [Hirani Ph.D. dissertation (2003)] for primal-primal wedge product:

The wedge product between a discrete primal 1-form α and a discrete primal 0-form β defined over a primal edge $[0, 1]$ is

$$\langle \alpha \wedge \beta, [0, 1] \rangle = \frac{1}{2} \langle \alpha, [0, 1] \rangle (\langle \beta, [0] \rangle + \langle \beta, [1] \rangle).$$

The discrete wedge product expression for the whole mesh:

$$\frac{1}{2} \begin{bmatrix} \alpha_0 & \alpha_0 & 0 & 0 \\ 0 & \alpha_1 & \alpha_1 & 0 \\ \alpha_2 & 0 & \alpha_2 & 0 \\ 0 & \alpha_3 & 0 & \alpha_3 \\ 0 & 0 & \alpha_4 & \alpha_4 \end{bmatrix} \begin{bmatrix} \beta_0 \\ \beta_1 \\ \beta_2 \\ \beta_3 \end{bmatrix}$$

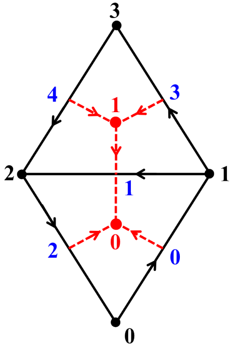

2D DEC discretization:

The discretization is carried out for the vorticity form of N-S equations.

$$\boxed{\frac{\partial \mathrm{d}\mathbf{u}^\flat}{\partial t} + (-1)^{N+1}\mu \mathrm{d} * \mathrm{d} * \mathrm{d}\mathbf{u}^\flat + (-1)^N \mathrm{d} * \left(\mathbf{u}^\flat \wedge *\mathrm{d}\mathbf{u}^\flat\right) = 0.}$$

$$\begin{tikzcd} C^0(K) \arrow[r, "\mathrm{d}_0"] \arrow[d, "*_0"] & C^1(K) \arrow[r, "\mathrm{d}_1"] \arrow[d, "*_1"] & C^2(K) \arrow[d, "*_2"] \\ D^2(\star K) & D^1(\star K) \arrow[l, "-\mathrm{d}_0^T"'] & D^0(\star K) \arrow[l, "\mathrm{d}_1^T"'] \end{tikzcd}$$

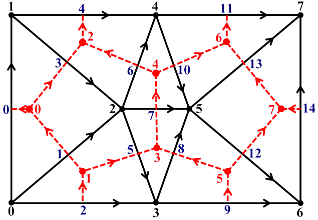

$$\boxed{\begin{aligned} -\mathrm{d}_0^T \frac{U^{n+1} - U^n}{\Delta t} &+ \mu \mathrm{d}_0^T *_1 \mathrm{d}_0 *_0^{-1} \left[-\mathrm{d}_0^T U + \mathrm{d}_b V\right] \\ &- \mathrm{d}_0^T *_1 W_v *_0^{-1} \left[-\mathrm{d}_0^T U + \mathrm{d}_b V\right] = 0. \end{aligned}}$$

2D DEC discretization: Cont.

$$\boxed{\begin{aligned}-\mathrm{d}_0^T\frac{U^{n+1}-U^n}{\Delta t}&+\mu\mathrm{d}_0^T\ast_1\mathrm{d}_0\ast_0^{-1}\left[-\mathrm{d}_0^T U+\mathrm{d}_b V\right]\\&-\mathrm{d}_0^T\ast_1 W_v\ast_0^{-1}\left[-\mathrm{d}_0^T U+\mathrm{d}_b V\right]=0.\end{aligned}}$$

Substitute with $U=\ast_1\mathrm{d}_0\Psi$

$$\boxed{\begin{aligned}-\frac{1}{\Delta t}\mathrm{d}_0^T\ast_1\mathrm{d}_0\Psi^{n+1}&-\mu\mathrm{d}_0^T\ast_1\mathrm{d}_0\ast_0^{-1}\mathrm{d}_0^T\ast_1\mathrm{d}_0\Psi\\&+\mathrm{d}_0^T\ast_1 W_v\ast_0^{-1}\mathrm{d}_0^T\ast_1\mathrm{d}_0\Psi=F.\end{aligned}}$$

$$F=\frac{1}{\Delta t}\mathrm{d}_0^T U^n-\mu\mathrm{d}_0^T\ast_1\mathrm{d}_0\ast_0^{-1}\mathrm{d}_b V+\mathrm{d}_0^T\ast_1 W_v\ast_0^{-1}\mathrm{d}_b V$$

2D DEC discretization: Cont.

The linear system is solved in two steps as a predictor-corrector method.

1. First, we advance the system explicitly by a half time step

$$\boxed{\begin{aligned}&\left[-\frac{1}{0.5\Delta t}\mathrm{d}_0^T *_1 \mathrm{d}_0\right]\Psi^{n+\frac{1}{2}}\\ &= F + \left[\mu \mathrm{d}_0^T *_1 \mathrm{d}_0 *_0^{-1} \mathrm{d}_0^T - \mathrm{d}_0^T *_1 W_v^n *_0^{-1} \mathrm{d}_0^T\right] U^n\end{aligned}}$$

$$\Psi^{n+\frac{1}{2}} \quad \Rightarrow \quad U^{n+\frac{1}{2}} = *_1 \mathrm{d}_0 \Psi^{n+\frac{1}{2}} \quad \Rightarrow \quad W_v^{n+\frac{1}{2}}$$

2. Then solve the linear system semi-implicitly

$$\boxed{\begin{aligned}&[-\frac{1}{\Delta t}\mathrm{d}_0^T *_1 \mathrm{d}_0 - \mu \mathrm{d}_0^T *_1 \mathrm{d}_0 *_0^{-1} \mathrm{d}_0^T *_1 \mathrm{d}_0\\ &+ \mathrm{d}_0^T *_1 W_v^{n+\frac{1}{2}} *_0^{-1} \mathrm{d}_0^T *_1 \mathrm{d}_0]\Psi^{n+1} = F\end{aligned}}$$

The evaluation of the tangential velocity at $(n + \frac{1}{2})$ was shown [Perot (2000)] to be necessary for kinetic energy conservation.

Conservation properties: Mass conservation

$$U = \ast_1 \mathrm{d}_0 \Psi$$

The discrete continuity equation is:

$$\ast_2 \mathrm{d}_1 \ast_1^{-1} U = 0$$

$$[\ast_2 \mathrm{d}_1 \ast_1^{-1}][\ast_1 \mathrm{d}_0]\Psi = \ast_2 \mathrm{d}_1 \mathrm{d}_0 \Psi = 0$$

The developed formulation guarantees the mass conservation up to the machine precision, regardless of the error incurred during the linear system solution.

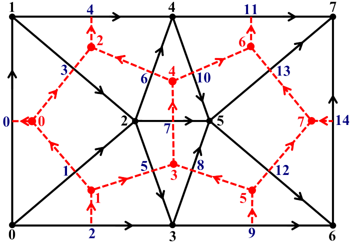

$$-\frac{\mathrm{d}_0^T U^{n+1} - \mathrm{d}_0^T U^n}{\Delta t} + \mu \mathrm{d}_0^T *_1 \mathrm{d}_0 *_0^{-1} [-\mathrm{d}_0^T U] - \mathrm{d}_0^T *_1 W_v *_0^{-1} [-\mathrm{d}_0^T U] = 0$$

$$-\frac{\mathrm{d}_0^T U^{n+1} - \mathrm{d}_0^T U^n}{\Delta t} + \mu \mathrm{d}_0^T [*_1 \mathrm{d}_0 X] - \mathrm{d}_0^T [*_1 W_v X] = 0$$

- The vorticity out-flux from a dual cell boundary is exactly equal to the vorticity in-flux to the neighboring dual cell.
- The vorticity is conserved locally and globally up to the machine precision.

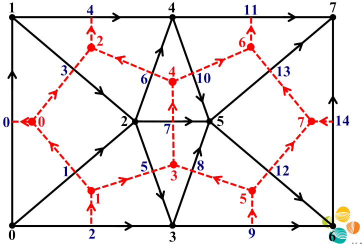

Test cases: Driven cavity

- The driven cavity flow is simulated at $Re = 1000$.
- The simulations are carried out on a Delaunay mesh and a structured-triangular mesh with 32482 and 32258 elements, respectively $\rightarrow$ almost the same resolution as a 128×128 Cartesian mesh.
- The time step $\Delta t = 0.1$, and the steady solution is attained at almost $T = 100$.

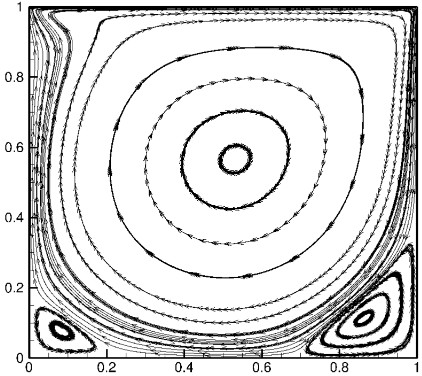

Test cases: Driven cavity

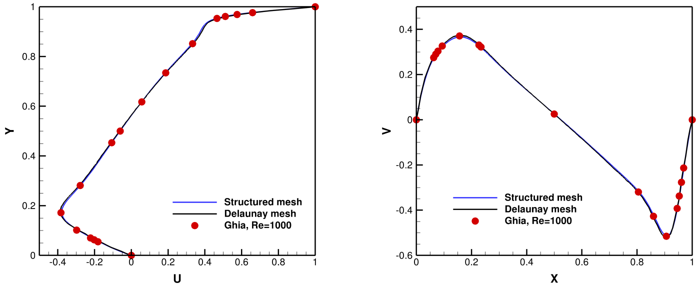

Figure: Cross-section of the steady velocity profile ($T = 100$) at the two domain center lines for driven cavity test case at Re $=$ 1000. The simulation results are compared with Ghia (1982).

Results: Taylor-Green vortices

- The decay of Taylor-Green vortices with time has an analytical solution that for the 2D case is expressed as

$$u_x = -\cos(x)\sin(y)e^{-2\nu t}$$
$$u_y = \sin(x)\cos(y)e^{-2\nu t}$$

- The simulation is conducted using a Delaunay mesh consisting of 50852 elements, a time step $\Delta t = 0.1$ and kinematic viscosity $\nu = 0.01$.
- Periodic boundary conditions applied on all domain boundaries.

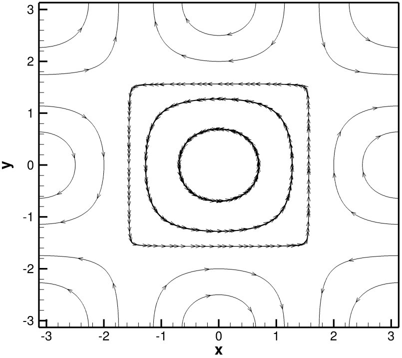

Results: Taylor-Green vortices

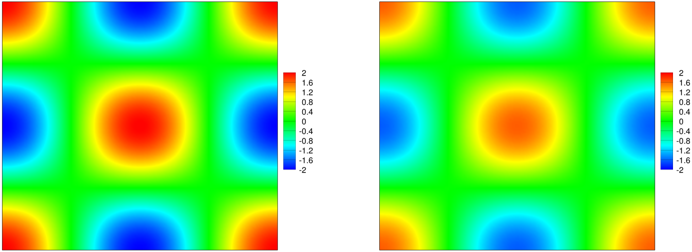

(a) (b)

Figure: The vorticity contour plot for Taylor-Green vortices at time (a) $T = 0$, (b) $T = 10$.

Results: Taylor-Green vortices

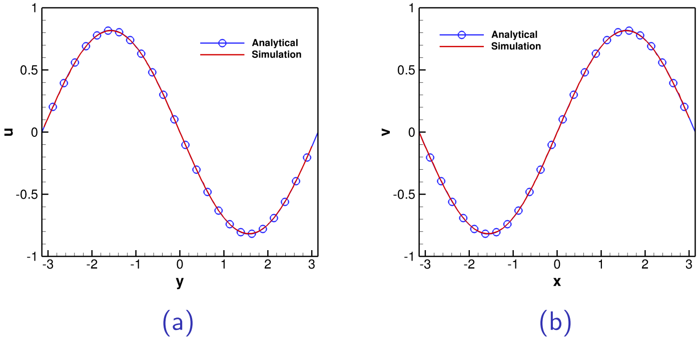

Figure: Cross-section of the velocity x and y-components profile at the two domain center lines for Taylor-Green vortices at time $T = 10$.

Test cases: Poiseuille flow

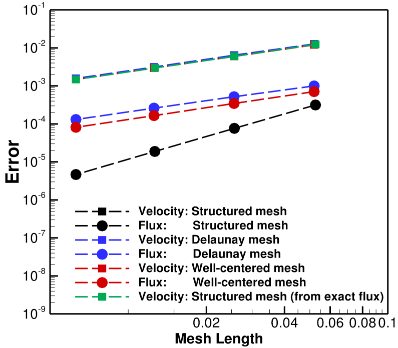

- The velocity 1-form u (flux) convergence is of a second order rate for the structured-triangular mesh case, and with a first order rate unstructured meshes.
- The velocity vector converges in the first order fashion due to its first order interpolation scheme.

Test cases: Double shear layer

- The initial flow for double shear layer represents a shear layer of finite thickness with a small magnitude of vertical velocity perturbation

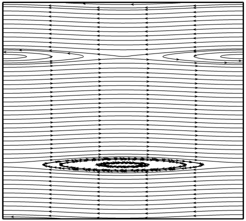

$$u_x = \begin{cases} \tanh((y-0.25)/\rho), & \text{for } y \leq 0.5, \\ \tanh((0.75-y)/\rho), & \text{for } y > 0.5, \end{cases}$$

$$u_y = \delta \sin(2\pi x)$$

with $\rho = 1/30$ and $\delta = 0.05$.

- The simulation is carried out for an inviscid flow ($\mu = 0$).
- Five simulations are conducted using a time step of $\Delta t = 0.001$ on structured-triangular meshes with number of elements equal to 3042, 12482, 32258, 50562 and 204800.
- Periodic boundary conditions applied on all domain boundaries.

Test cases: Double shear layer

Test cases: Double shear layer

- The kinetic energy is calculated as $\int_\Omega \mathbf{u}.\mathbf{u}\ d\Omega$.
- The relative kinetic energy error $(\frac{KE(0)-KE(T)}{KE(0)})$ is calculated at simulation time $T = 2.0$.

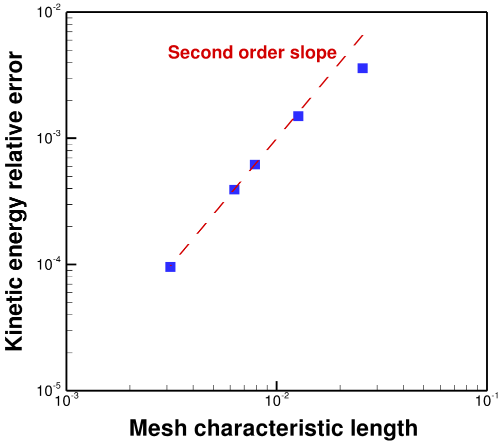

Results: Vortex leapfrogging

Test cases: Taylor vortices

- The vorticity distribution for each Taylor vortex is expressed as [A. McKenzie, PhD Dissertation, Caltech (2007)]

$$\omega(x,y) = \frac{G}{a}\left(2 - \frac{r^2}{a^2}\right)\exp\left(0.5\left(1 - \frac{r^2}{a^2}\right)\right)$$

with $G = 1.0$, $a = 0.3$.

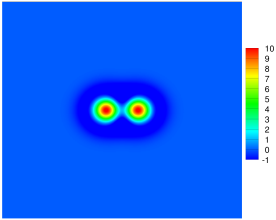

- The domain is initialized with two vortices separated by a distance of 0.8.
  - The simulations are carried out for an inviscid flow ($\mu = 0$) on a mesh consisting of 132204 equilateral triangular element, using various time steps in the range $[1.0 - 0.002]$.
  - Periodic boundary conditions applied on all domain boundaries.

The relative kinetic energy error ($\frac{KE(0)-KE(T)}{KE(0)}$) is calculated at simulation time $T = 20.0$.

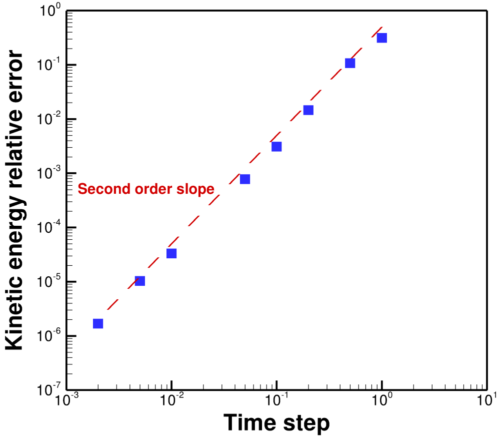

- A unit sphere surface is initialized with two vortices, separated by a distance of 0.4, having the distribution

$$\omega(x,y) = \frac{G}{a}\left(2 - \frac{r^2}{a^2}\right)\exp\left(0.5\left(1 - \frac{r^2}{a^2}\right)\right)$$

with $G = 0.5$, $a = 0.1$.

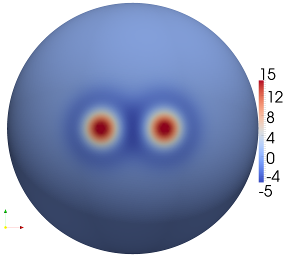

- The simulation is carried out for an inviscid flow ($\mu = 0$) using a mesh containing 327680 triangular elements, with various time steps in the range $[1.0 - 0.05]$.

Test cases: Taylor vortices on a spherical surface

The relative kinetic energy error ($\frac{KE(0)-KE(T)}{KE(0)}$) is calculated at simulation time $T = 10.0$.

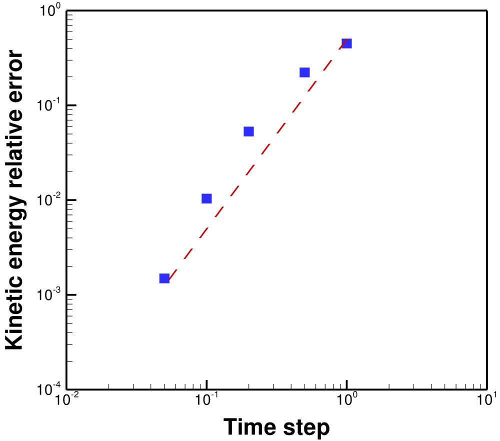

Results: Vortices ring on a spherical surface

- Consider N equidistant point vortices, having the same strength, positioned on a circle with fixed latitude on a spherical surface [Polvani et. al (1993)].
- It was shown analytically that the vortices will rotate around the z-axis in a stable fashion given that the circle's latitude $\theta < \theta_c$ and the number of vortices $N \leq 7$.
- For $N = 6$, the critical polar angle $\theta_c \sim 0.464$.

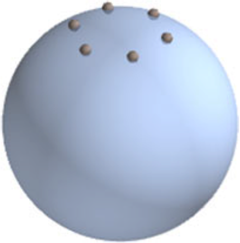

Figure: [Vankerschaver et. al (2014)]

Results: Vortices ring on a spherical surface

- The point vortices are replaced with vortices having the distribution

$$\omega = \frac{\tau}{cosh^2(\frac{3r}{a})}$$

with $\tau = 3.0$ to be the vortex strength, $a = 0.15$ is the vortex radius.

- The vortices are placed on a unit sphere at latitude $\theta = 0.4$.
- The spherical surface is meshed with 81920 elements, and the simulation is conducted for an inviscid flow ($\mu = 0$) with a time step $\Delta t = 0.005$.

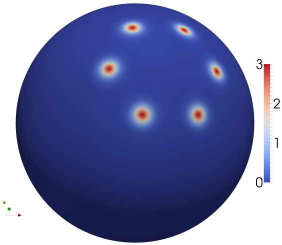

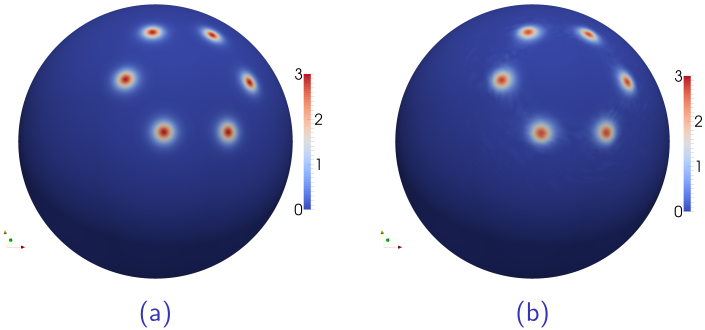

Figure: The vorticity contour plot for 6 vortices on a spherical surface at latitude $\theta = 0.4$ at time: (a) T=0.0 and (b) T=36.0.

The cyclic motion of the vortices can be captured by monitoring the relative solution change ($\frac{||U(t)-U(0)||}{||U(0)||}$) w.r.t. the initial solution.

Results: Vortices ring on a spherical surface

The relative solution change ($\frac{\|U(t)-U(0)\|}{\|U(0)\|}$).

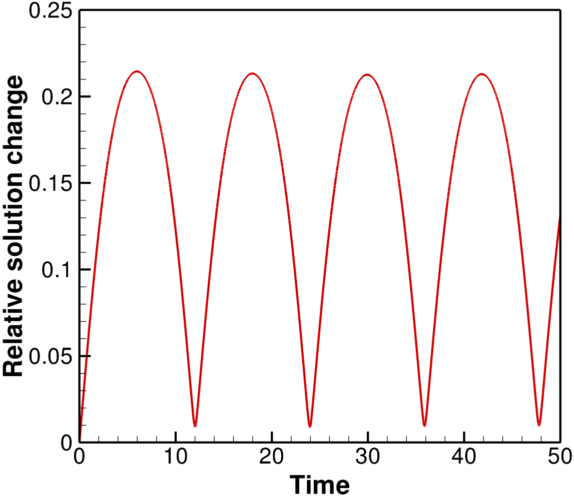

Results: Vortices ring on a spherical surface

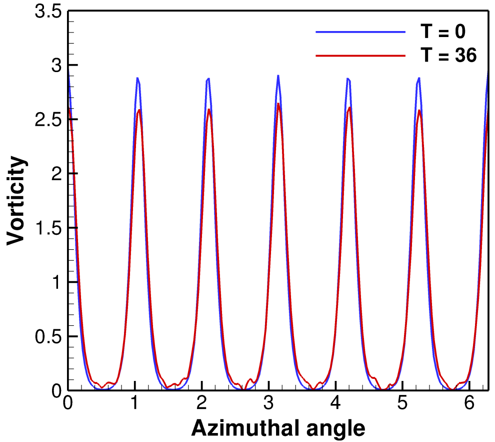

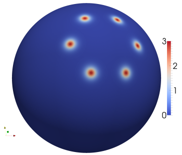

The relative change in the kinetic energy at time $T = 36$ is $\frac{KE(T{=}0) - KE(T{=}36)}{KE(T{=}0)} = 9.0 \times 10^{-6}$.

Test cases: Flow past a cylinder, Re = 40

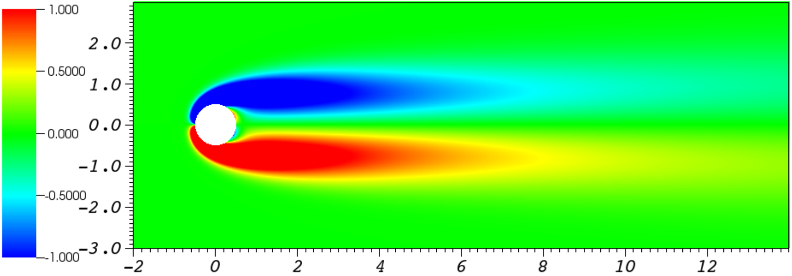

Figure: The vorticity contour plot, Re = 40.

Test cases: Flow past a cylinder, Re = 40

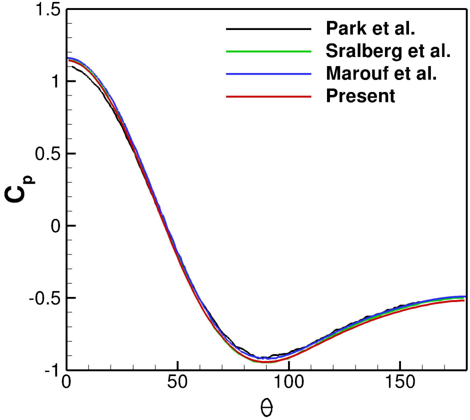

Figure: The pressure coefficient calculated on the cylinder surface.

Test cases: Flow past a cylinder, Re = 40

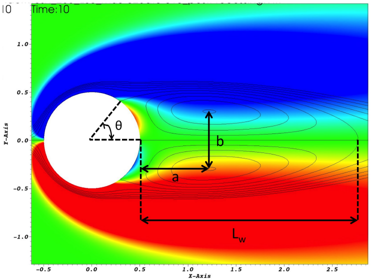

Reference	C_D	L_W	a	b	θ
Chiu et al.	1.52	2.27	0.73	0.60	53.6
Gautier et al.	1.49	2.24	0.71	0.59	53.6
Brehm et al.	1.51	2.26	0.72	0.58	52.9
Marouf et al.	1.54	2.25	0.71	0.59	53.7
Present	1.51	2.26	0.72	0.60	53.8

Test cases: Flow past a cylinder, Re = 100

Test cases: Flow past a cylinder, Re = 100

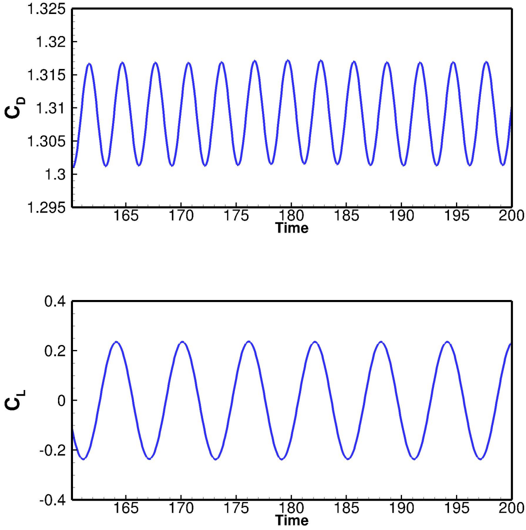

Figure: The drag and lift coefficients calculated on the cylinder surface

Drag coefficient and the Strouhal number for the flow over a circular cylinder at Re $= 100$.

Reference	C_D	S_t
Chiu et al.	1.35 ± 0.0120	0.167
Le et al.	1.37 ± 0.0090	0.160
Brehm et al.	1.32 ± 0.0100	0.165
Russell and Wang	1.38 ± 0.0070	0.172
Liu et al.	1.35 ± 0.0120	0.165
Marouf et al.	1.34 ± 0.0089	0.166
Present	1.31 ± 0.0080	0.175

We are currently trying finer meshes and bigger domains.

KAUST
King Abdullah University of Science and Technology

Hodge star operators for non-Delaunay meshes:

- DEC discretizations require a dual mesh, which is usually circumcentric.
- The circumcentric dual mesh is well-defined only on Delaunay meshes.

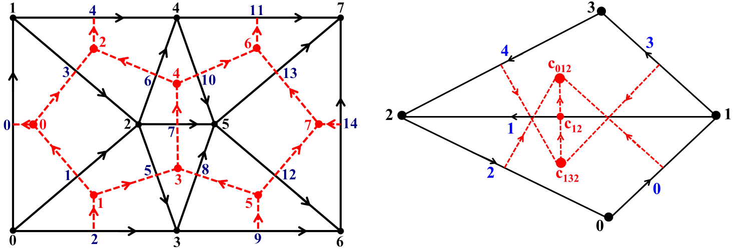

(a) (b)

Figure: The circumcentric dual mesh defined on (a) Delaunay, and (b) non-Delaunay simplicial mesh.

For non-Delaunay meshes, a barycentric dual mesh can be used.

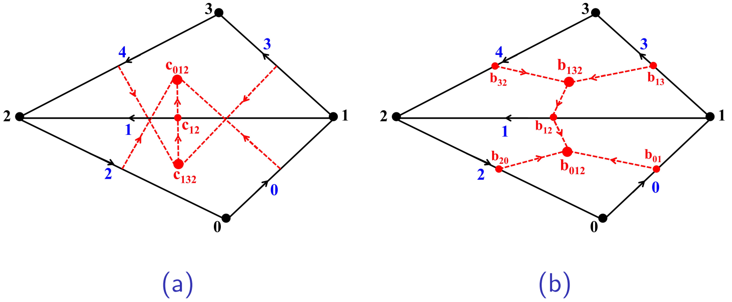

Figure: A non-Delaunay simplicial mesh with (a) circumcentric, and (b) barycentric dual mesh.

Which Hodge star operators need redefinition?

$$\begin{tikzcd}
C^0(K) \arrow[r, "\mathrm{d}_0"] \arrow[d, "*_0"] & C^1(K) \arrow[r, "\mathrm{d}_1"] \arrow[d, "*_1"] & C^2(K) \arrow[d, "*_2"] \\
D^2(\star K) & D^1(\star K) \arrow[l, "-\mathrm{d}_0^T"'] & D^0(\star K) \arrow[l, "\mathrm{d}_1^T"']
\end{tikzcd}$$

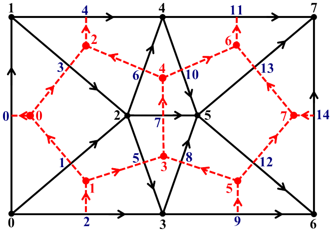

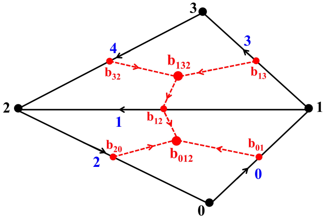

- The Hodge star operators that need to be redefined are $*_1$ and its inverse $*_1^{-1}$.
- We focus here only at the discrete operator $*_1$.

Discrete definitions for the Hodge operator $*_1$:

- The circumcentric definition:

$$\boxed{[*_1]^C_{ii} = \frac{|\star\, \sigma^1_i|}{|\sigma^1_i|}.}$$

- The Galerkin definition:

$$\boxed{[*_1]^G_{ij} = \int_{\sigma^2} \left\langle W^{(\sigma^2)}_{\sigma^1_i}, W^{(\sigma^2)}_{\sigma^1_j} \right\rangle \alpha.}$$

$$W^{(\sigma^2)}_{[v_i,v_j]} = \mu_i \, \mathrm{d}\mu_j - \mu_j \, \mathrm{d}\mu_i.$$

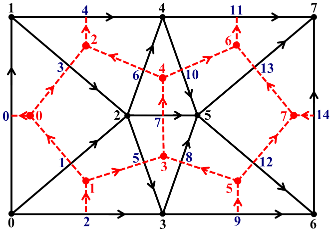

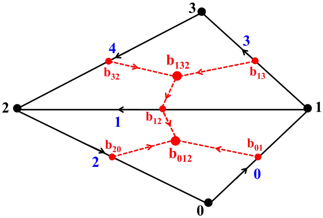

The barycentric definition: [Auchmann & Kurz (2006)]

$$u^{(\sigma^2)} = \sum_{\sigma_i^1 \prec \sigma^2} u_{\sigma_i^1} W_{\sigma_i^1}^{(\sigma^2)}.$$

$$w^{(\sigma^2)} = * u^{(\sigma^2)} = \sum_{\sigma_i^1 \prec \sigma^2} u_{\sigma_i^1} * W_{\sigma_i^1}^{(\sigma^2)}$$

$$= \sum_{\sigma_i^1 \prec \sigma^2} u_{\sigma_i^1} W_{\sigma_i^1}^{(\sigma^2)*}.$$

$$w_{\star\sigma_i^1} = \sum_{\sigma_k^2} \sum_{\sigma_j^1 \prec \sigma_k^2} u_{\sigma_j^1} W_{\sigma_j^1}^{(\sigma_k^2)*} (\star\sigma_i^1 \cap \sigma_k^2).$$

$$\left\langle \star\sigma_i^1 \cap \sigma_k^2, \mathbf{x} \right\rangle = |\sigma_k^2| \, W_{\sigma_i^1}^{(\sigma_k^2)*}(\mathbf{x}).$$

$$\boxed{[*_1]_{ij}^B = |\sigma^2| \left\langle W_{\sigma_i^1}^{(\sigma^2)*}, W_{\sigma_j^1}^{(\sigma^2)*} \right\rangle.}$$

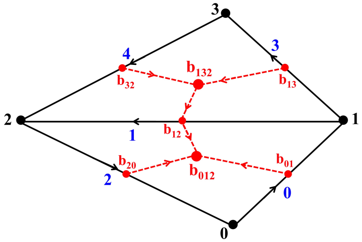

Numerical experiments:

- Convergence tests are carried out for scalar Poisson and incompressible Navier-Stokes equations solutions in 2D.
- The simulations are carried out for:
  1. Five unstructured Delaunay meshes (created independently).
  2. Sequence of five sequentially divided non-Delaunay meshes.
  3. Five structured-triangular meshes (isosceles right triangles).
  4. Five highly-distorted non-Delaunay meshes.
- The experiments compare the circumcentric, the Galerkin, and the barycentric Hodge operators.

Sample meshes:

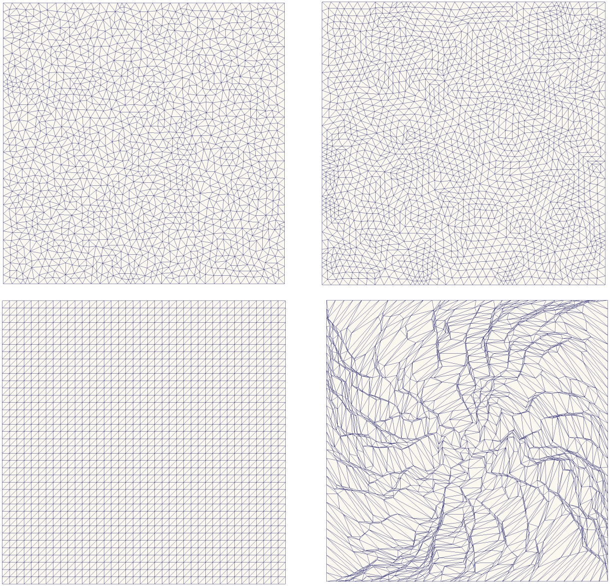

Scalar Poisson equation:

Solve $\boxed{\star_0^{-1}[-\mathrm{d}_0^T]\,\star_1\,\mathrm{d}_0 p = \phi}$, p is defined on the primal nodes.

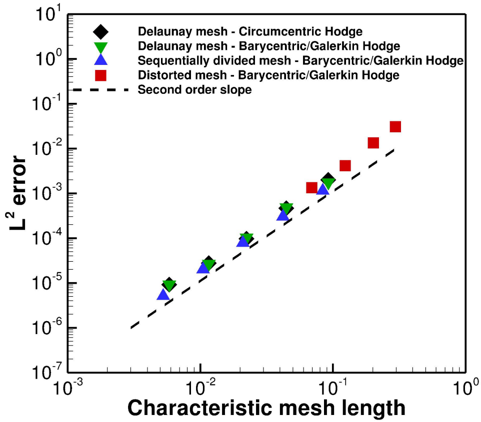

Figure: The numerical convergence of the L^2 error of p for the scalar Poisson Eq. with Neumann boundary conditions.

Incompressible Navier-Stokes:

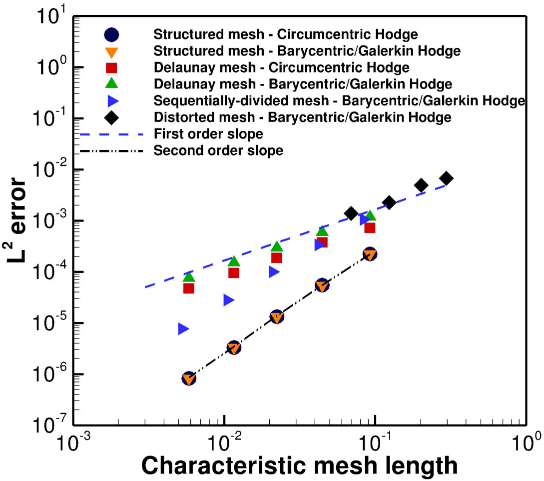

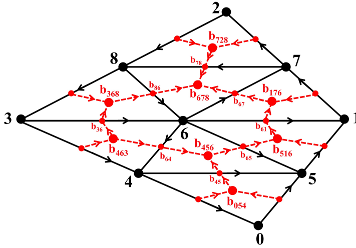

The computational cost:

The increase in the computational cost is moderate.

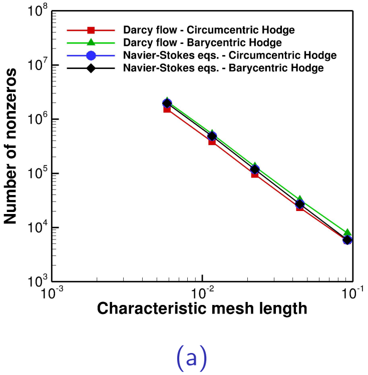

Figure: (a) The number of non-zeros in the global matrices. (b) The solution time (in seconds) for various mesh sizes.

The limitations of the barycentric Hodge operator:

- The barycentric Hodge operator $*_1$ has almost five nonzero entries in each row. Therefore, its inverse operator $*_1^{-1}$ will not be sparse.
- The inverse Hodge star operator $*_1^{-1}$ is required to solve:
  - The incompressible N-S equations using velocity-pressure formulation.
  - The scalar Poisson equation to calculate the pressure in incompressible N-S solutions.
  - The incompressible single fluid resistive MHD equations.
- The DEC solution of such problems is currently limited to Delaunay meshes (with circumcentric dual).

KAUST
King Abdullah University of Science and Technology

Hybrid discrete Hodge star operator:

- Even for domains with complex geometry, it is not difficult to generate high quality mesh that, even if was subdivided, most of its triangles will remain Delaunay.

- Proposal: Use a hybrid dual mesh

Hybrid dual mesh:

Only two pairs of triangle are non-Delaunay.

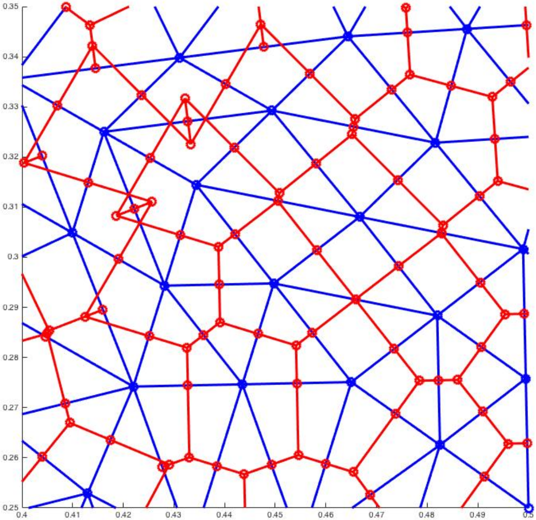

Hybrid dual mesh:

Only for these non-Delaunay triangles, changes to barycentric.

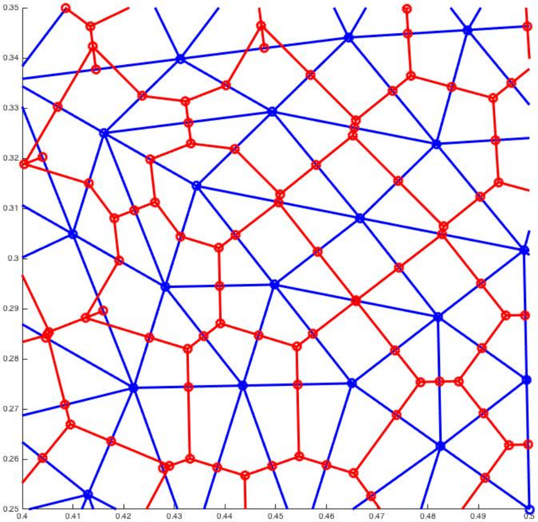

Hybrid dual mesh:

Change also for some of the neighbors.

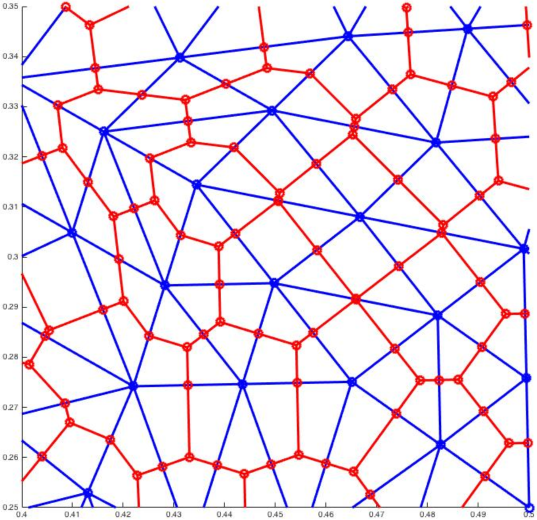

The hybrid Hodge star operator $*_1$:

- For Edges that have a circumcentric dual edge:

$$\boxed{[*_1]^H_{ii} = \frac{|\star\sigma^1_i|}{|\sigma^1_i|}.}$$

- Otherwise, interpolate through Whitney maps:

$$\boxed{[*_1]^H_{ij} = \sum_{\sigma^2_k} W^{(\sigma^2_k)*}_{\sigma^1_j}(\star\sigma^1_i \cap \sigma^2_k),}$$

where the summation is over the triangles σ^2_k neighbor to the edge σ^1_i.

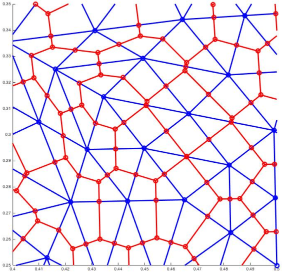

KAUST
King Abdullah University of Science and Technology

- The hybrid Hodge star operator can be represented as:

$$[*_1]^H = \left[\begin{array}{c|cc} D_0 & \multicolumn{2}{c}{0} \\ \hline 0 & D_1 & 0 \\ \cline{2-3} & M_0 & M_1 \end{array}\right]$$

- The inverse matrix $*_1^{-1}$ can then be computed as:

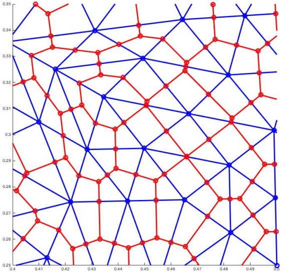

$$[*_1^{-1}]^H = \left[\begin{array}{c|cc} D_0^{-1} & \multicolumn{2}{c}{0} \\ \hline 0 & D_1^{-1} & 0 \\ \cline{2-3} & -M_1^{-1} M_0 D_1^{-1} & M_1^{-1} \end{array}\right]$$

KAUST
King Abdullah University of Science and Technology

- We start with Delaunay mesh.
- Select a random edge, move the neighbor triangles apexes towards the edge's midpoint till the triangles pair become non-Delaunay.
- Repeat until a specific ratio of edges with non-Delaunay triangles pair is reached.

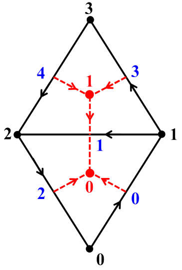

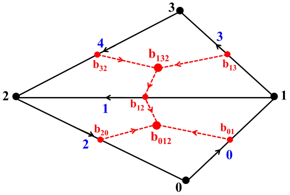

Test meshes:

	Edges with non-Delaunay triangles pair	Edges interpolated using Whitney based interpolation
non-Delaunay mesh 1	1%	$\sim$ 6%
non-Delaunay mesh 2	2%	$\sim$ 13%
non-Delaunay mesh 3	5%	$\sim$ 32%
non-Delaunay mesh 4	7%	$\sim$ 43%

Convergence of the hybrid Hodge operator $\star_1$:

Solving the incompressible N-S equation:

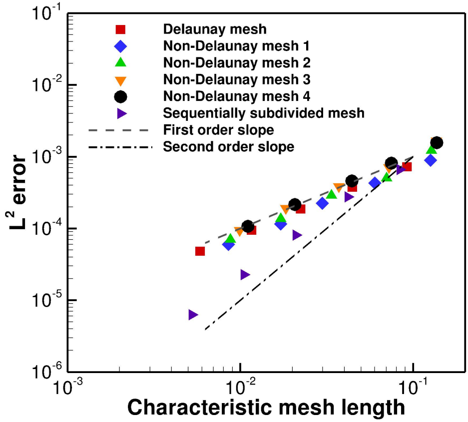

Figure: The numerical convergence of the L^2 error of the velocity 1-form.

Convergence of the hybrid Hodge operator $\star_1$:

Solve $\boxed{\star_0^{-1}[-\mathrm{d}_0^T]\,\star_1\,\mathrm{d}_0 p = \phi}$, p is defined on the primal nodes.

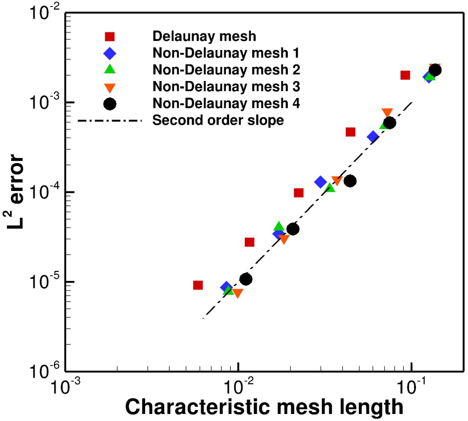

Figure: The numerical convergence of the L^2 error of p for the scalar Poisson Eq. with Neumann boundary conditions.

Convergence of the inverse hybrid Hodge operator $\star_1^{-1}$:

Solve $\boxed{\star_2 \mathrm{d}_1 \star_1^{-1} \mathrm{d}_1^T p = \phi}$, p is defined on the dual nodes.

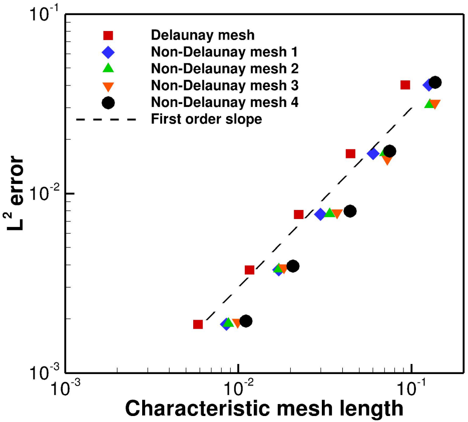

Figure: The numerical convergence of the L^2 error of p for the scalar Poisson Eq. with Neumann boundary conditions.

The % matrix density $= \dfrac{\text{no. of nonzero entries}}{\text{total number of matrix entries}} \times 100$

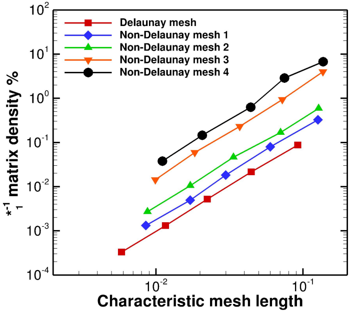

(a)

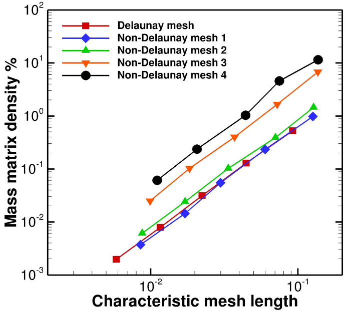

(b)

Figure: The % matrix density of the (a) the $\star_1^{-1}$ matrix, and (b) the global mass matrix.

The solution time:

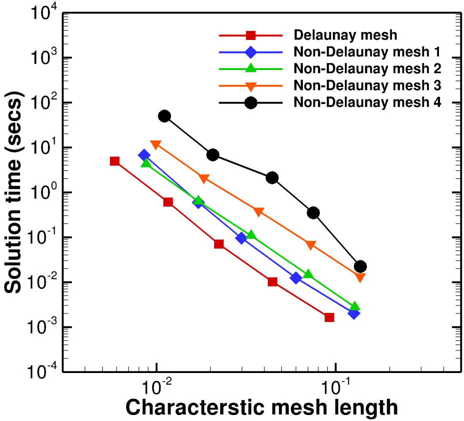

Figure: The scalar Poisson equation solution time in seconds.

KAUST
King Abdullah University of Science and Technology

DEC discretization of MHD equations:

The governing equations for single-fluid resistive magnetohydrodynamics are:

$$\frac{\partial \mathbf{u}}{\partial t} - \frac{1}{Re}\Delta \mathbf{u} + (\mathbf{u}.\nabla)\mathbf{u} + \nabla p + \mathbf{B} \times (\nabla \times \mathbf{B}) = 0,$$

$$\frac{\partial \mathbf{B}}{\partial t} - \frac{1}{Re\ Pm}\Delta \mathbf{B} - \nabla \times (\mathbf{u} \times \mathbf{B}) = 0,$$

$$\nabla.\mathbf{u} = 0,$$

$$\nabla.\mathbf{B} = 0,$$

MHD equations in exterior calculus notation:

The equations in exterior calculus notation in 2D are:

$$
\begin{aligned}
\frac{\partial \mathbf{u}^\flat}{\partial t} - \frac{1}{Re} * \mathrm{d} * \mathrm{d}\mathbf{u}^\flat &+ *(\mathbf{u}^\flat \wedge *\mathrm{d}\mathbf{u}^\flat) \\
&- *(*\mathbf{B}^\flat \wedge *\mathrm{d} * \mathbf{B}^\flat) + \mathrm{d}p^d = 0, \\
\frac{\partial \mathbf{B}^\flat}{\partial t} - \frac{1}{Re\ Pm}\mathrm{d} * \mathrm{d} * \mathbf{B}^\flat &+ \mathrm{d} * (\mathbf{u}^\flat \wedge *\mathbf{B}^\flat) = 0, \\
&* \mathrm{d} * \mathbf{u}^\flat = 0, \\
&* \mathrm{d} * \mathbf{B}^\flat = 0.
\end{aligned}
$$

KAUST
King Abdullah University of Science and Technology

DEC discretization of MHD equations:

- Define u and v as the discrete dual and primal 1-forms.
- Define B and b as the discrete primal and dual 1-forms.

$$\frac{\partial u}{\partial t} - \frac{1}{Re} \ast_1 \mathrm{d}_0 \ast_0^{-1} [-\mathrm{d}_0^T] u + \ast_1 (v \wedge \ast_0^{-1} [-\mathrm{d}_0^T] u)$$

$$- \ast_1 (\boxed{\ast_1^{-1}} b \wedge \ast_0^{-1} [-\mathrm{d}_0^T] \ast_1 B) + \mathrm{d}_1^T p^d = 0$$

$$\frac{\partial B}{\partial t} - \frac{1}{Re\ Pm} \mathrm{d}_0 \ast_0^{-1} [-\mathrm{d}_0^T] \ast_1 B + \mathrm{d}_0 \ast_0^{-1} (u \wedge \ast_1 B) = 0,$$

$$\ast_2 \mathrm{d}_1 \boxed{\ast_1^{-1}} u = 0,$$

$$\ast_2 \mathrm{d}_1 B = 0.$$

KAUST
King Abdullah University of Science and Technology

Conclusions

- A conservative discretization for NS equations was derived using DEC.
- The scheme converges with second order for structured/semi-structured meshes, and first order for otherwise unstructured meshes.
- The mass and vorticity were conserved up to machine precision for all conducted test cases.
- The kinetic energy converges with second order with the mesh size and time step for the tested cases on structured/semi-structured meshes.

KAUST
King Abdullah University of Science and Technology

Conclusions:

- A comparison between the circumcentric Hodge operator versus the Galerkin and the barycentric Hodge operators on surface simplicial meshes was presented.
- The Galerkin and the barycentric Hodge operators reproduce the convergence order of the circumcentric Hodge for both Darcy flow and incompressible Navier-Stokes solutions.
- A super-convergence behavior (almost second order) was observed when using the barycentric Hodge star on a sequence of non-Delaunay unstructured meshes generated through sequential mesh subdivision.
- In terms of the computational cost, the DEC solutions exhibit a modest decrease in the linear system sparsity when using the barycentric Hodge star operator.

KAUST
King Abdullah University of Science and Technology

Conclusions:

- A hybrid dual mesh is employed for meshes having relatively small fraction of non-Delaunay triangles.
- The hybrid Hodge star operator $\star_1$ converges as expected.
- The inverse hybrid Hodge star operator $\star_1^{-1}$ converges even with relatively high ratio of non-Delaunay triangles.

- Preliminary DEC discretization of single fluid resistive MHD presented.

Acknowledgment:

This research was supported by the KAUST Office of Competitive Research Funds under Award No. URF/1/1401-01-01.

THANK YOU